



Full Length Article

Comprehensive adhesion model based on the surface characteristics of the coal particles

Fanfei Lin, Zhongjie Shen, Qinfeng Liang, Zhenghua Dai, Jianliang Xu*, Haifeng Liu*

Shanghai Engineering Research Center of Coal Gasification, East China University of Science and Technology, P.O. Box 272, Shanghai 200237, PR China
Institute of Clean Coal Technology, East China University of Science and Technology, P. O. Box 272, Shanghai 200237, PR China



ARTICLE INFO

Keywords:

Particle deposition
Surface characteristics
Critical kinetic energy
Ash melting fraction

ABSTRACT

A comprehensive model for the adhesion of coal ash or char particle was established in this study, which includes the particles' properties and slag layer. The physical properties of the particles include their kinetic parameters and surface characteristics. The particle surface characteristics, such as particle ash ratio and melting fraction, play an important role in particle adhesion. A sub-model of adhesion probability, constructed based on particle surface properties, was also introduced as a part of this comprehensive model. The particle adhesion propensity was determined by considering the kinetic energy criterion of the particles. The model was validated using two sets of particle deposition experiments at different temperatures. Discussion of the model shows that, when the particle kinetic energy is within the medium range, more significant than the critical velocity and less than the critical kinetic energy required to overcome viscosity or surface tension, the particle adhesion is determined by the probability corresponding to the surface characteristics. Furthermore, it is found that the adhesion probability increases with ash-carbon ratio and carbon conversion, and exhibits different trends above and below the flow temperature.

1. Introduction

In the process of coal utilization, slag discharge or ash accumulation inevitably occurs in the furnace. Reducing ash deposition in the boilers is needed in order to improve the heat exchange effect. For gasifiers, molten ash deposition contributes to the formation of a slag layer that protects the membrane wall [1]. Therefore, it is necessary to investigate the particle deposition process in the furnace.

The ash deposition process consists of transportation and adhesion [2]. Particle transportation is mainly controlled by gas–solid two-phase flow. The process of particle adhesion depends not only on the movement behavior but also on the surface properties of the particles. Experimental studies reveal that various factors can influence the ash deposition process, including the furnace temperature, ash melting characteristics, wall temperature, particles size and velocity [3–5], and carbon conversion [6]. To study the impact of these factors, several models have been proposed for particle adhesion [7]. The earlier models consider only a single factor such as critical viscosity [3], melting fraction [8], or establish the energy conservation model of the impact process, by assuming the particles are droplets [9,10]. In the subsequent studies, multiple factors have been considered. Kleinhans et al. [11,12]

proposed a model in which the critical viscosity was a function of the particle kinetic energy. Brink et al. [13] simultaneously considered two parameters of particle viscosity and melting fraction. Yang et al. [14] proposed an exponential relationship between the adhesion efficiency and residual energy from the surface energy, considering partial adhesion behavior and ash melting fraction of the slag layer. A more meticulous approach is to propose a comprehensive model for different conditions. Segmented models have been proposed based on the particles' temperature as well as the deposition surface [15,16]. When the temperature is smaller than the ash fusion temperature (AFT), the energy conservation model is adopted; otherwise, the adhesion probability is determined based on the melting fraction. In high temperature furnaces (i.e., entrained-flow gasifiers) where the temperature is above the ash flow temperature, the properties of liquid slag layer and carbon conversion are more significant [1,17]. For such conditions, a multi-factor model that includes wall and particle properties could be established. For example, Yong et al. [18] used three criteria of T_{CV} corresponding to the critical viscosity of the slag flow, critical Weber number, and critical carbon conversion for their modeling exercise. However, these Boolean criteria have been used without mechanism analysis or quantitative description of the adhesion process, thus resulting in poor reliability of the developed models. Troiano et al. [2] proposed a

* Corresponding authors.

E-mail addresses: xujl@ecust.edu.cn (J. Xu), hfliu@ecust.edu.cn (H. Liu).

<https://doi.org/10.1016/j.fuel.2022.123219>

Received 30 August 2021; Received in revised form 21 November 2021; Accepted 9 January 2022

Available online 18 January 2022

0016-2361/© 2022 Elsevier Ltd. All rights reserved.

Nomenclature			
A, a	ash content (mass fraction) in raw coal and particle	$P_{\mu,w}$	adhesion probability of corresponding to critical viscosity of wall
C, c	carbon content (mass fraction) in raw coal and particle	$r_{a/c}$	ash-carbon ratio
d_p, d_M	particle diameter and the maximum spreading diameter	T_i, T_M	the temperature of initial melting and liquid phase fraction is 0.9
E_k, E_s	kinetic energy and surface energy of the particle	u_p, u_{cr}	velocity and critical velocity of the particle
$E_{k,c}, E_{k,c}^*$	critical kinetic energy and its dimensionless number of the particle	$u_{g,t}, u_{tc}$	wall shear velocity and critical shear velocity of the gas
$E_{k,c,\mu}, E_{k,c,\gamma}$	critical kinetic energy corresponding to viscosity and surface tension	v_a	volume fraction of ash in the particle
e	residual kinetic energy	W	adhesion work
$f_M, f_{M,w}$	ash melting fraction of particle and wall	X	carbon conversion
f_C	adhesion probability base on carbon conversion	φ	impact angle
P_p, P_w, P_T	adhesion probability of the particle, wall, and the total.	θ	contact angle
p_S, p_K	adhesion probability of surface characteristics and particle kinetic parameters	μ_p, μ_w	viscosity of the particle and wall
		γ_p	surface tension of the particle
		ξ_m	maximum spread ratio

different approach and started from a macroscopic perspective. They used the coefficient of restitution as well as the relationship between the incident velocity and the amount of residual carbon as parameters to establish a connection with deposition mass fraction. However, this approach still needs further development.

The above studies indicate that molten slag/droplet viscosity, ash melting fraction, kinetic energy, and surface tension are the parameters that have been considered in current particle adhesion models. However, according to Xu's research on gasifiers [19], the particles captured after impacting the wall were not entirely converted, and contained residual carbon, which could have been ignored or simplified in most of the developed models. Liu et al. [20,21] conducted in-situ experimental research on coal char particle gasification, and examined the morphological characteristics of the particles during the reaction processes; hence, they proposed several char-slag interaction modes. It is conducive to establishing a relationship between the residual carbon and adhesion propensity. In industrial gasifiers and boilers, it was found that the particle surface characteristics exhibited a significant influence on the particle deposition process. To properly describe the particle adhesion process on membrane wall and accurately predict the particle deposition rate, we constructed a particle adhesion model based on these surface characteristics. In this model, the effects of two important parameters (i.e., carbon conversion and melting fraction) on different morphology characteristics of the particles were studied. Furthermore, a comprehensive adhesion probability model was proposed based on the kinetic energy, viscosity and surface tension of the particles.

2. Comprehensive adhesion model

The process of particle adhesion is complex. On one hand, the kinetic energy and physical properties of the particles can affect this process. On the other hand, the influence of slag layer on the wall surface cannot be ignored. Therefore, the properties of the particles as well as the slag layer should be considered in order to develop a comprehensive particle adhesion model.

2.1. Particle adhesion model P_p

The particles injected from a nozzle undergo complex chemical reactions, heat transfer, and phase transformation in the furnace. Therefore, their properties often vary when they contact the wall, which results in different adhesion propensities. According to the literature, the adhesion process is affected by the relationship between the physical properties (i.e., viscosity and surface tension) and kinetic energy of the particles, assuming that the particles are liquid [11,14]. When the

particles are solid, they deposit the critical velocity according to the mature impact theory [22]. In addition, the experimental studies prove that the surface characteristics of the particles vary at different temperatures and conversion states [20,21,23,24], which can be used to determine particle adhesion.

Based on the above analysis, the particle adhesion criteria can be summarized in the form of two elements: surface characteristics and kinetic parameters. Each element represents the adhesion probability or sticking propensity corresponding to that element alone:

$$P_p = F(p_S, p_K) \tag{1}$$

where p_S and p_K represent the adhesion probability functions corresponding to the surface characteristics and kinetic parameters, respectively. The models representing these two adhesion probability functions are described in the following two sections.

2.1.1. Adhesion sub-model based on the surface characteristics

According to the in-situ studies of surface morphology evolution of the particles conducted with high-temperature stage microscope, the residual carbon/ash solid aggregate and a liquid phase (i.e., the melting of ash content) is formed on the particle surface transformed during motion [20,23]. Since the melted ash component could facilitate particle adhesion, the state of melting ash and its distribution was used to describe the adhesion propensity of the particles. The former is the ash melt fraction, and the latter is related to the conversion state of the particles [20]. As shown in Fig. 1, the adhesion properties of the solid particle and liquid droplet had been abundantly studied. The particle states can be divided into 7 types according to two variables. In this work, the adhesion propensity of the melted particles with residual carbon was modeled.

Temperature is an important parameter affecting the particle's

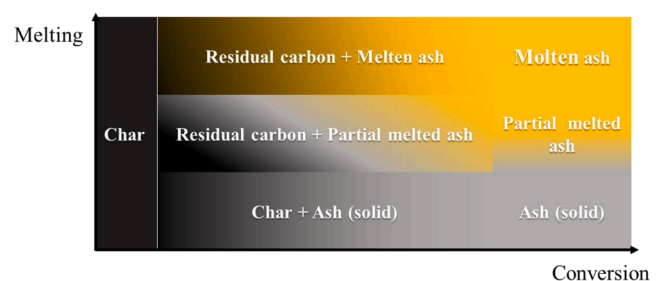


Fig. 1. Different states of the particles with the degree of conversion and melting as variables.

adhesion characteristics. In this study, the initial melting temperature T_i was introduced, and defined according to the initial temperature of the liquid phase curve calculated by FactSage [25]. It is assumed that at temperatures below T_i , the particles are solid and their surface properties do not affect the particle deposition characteristics. On the other hand, when the particle temperature is greater than T_i , the surface characteristics-based particle adhesion probability is determined by two factors:

$$p_s = F(f_M, f_c) (T_p \geq T_i) \quad (2)$$

where f_M represents the melting fraction, and f_c represents the adhesion probability based on the conversion.

(1) Ash melting fraction

According to Zhou's research on the sub-particle size of the coal ash, the fluctuating behavior of the elements on the surface of the coal ash leads to partial melting of the ash, which provides a basis for the adhesion of ash particles below the Ash Fusion Temperature (AFT) [23,24]. The liquid phase curve simulated by FactSage can be used as the melting fraction. The liquid phase curve of SH coal ash (based on SlagA) is shown in Fig. 2. By fitting the liquid phase curve, the ash melting fraction can be expressed as a function of particle temperature:

(2) Adhesion probability based on the carbon conversion

The existing ash adhesion models generally ignore the effect of residual carbon on particle deposition [11,14]. However, as shown in Fig. 3, the morphologies of the particles significantly vary with carbon conversion [20,21]. The initial distribution of ash in coal char is randomly dispersed in the form of plum pudding mode (Fig. 3(a)). When the temperature of the particles is lower than that of the ash flow temperature (FT) and the ash content is still in the molten (or partial molten) state [23], a muffin-like structure appears at the surface of the particles (Fig. 3(b)). As the reaction progresses, the slag layer will completely wrap the particles to finally form a watermelon pattern (Fig. 3(c)). When the ash content is high enough and the particle temperature is greater than the ash flow temperature, the residual carbon is suspended at the surface of the molten-slag droplet (Fig. 3(d)).

Based on the above evolution characteristics of molten slag particle morphologies, it can be inferred that the particle morphology is closely related to temperature and ash content. Generally, FT is close to the temperature corresponding to the simulated liquid phase fraction of 0.9, or denoted as T_M . These characteristics can be considered in two cases according to T_M .

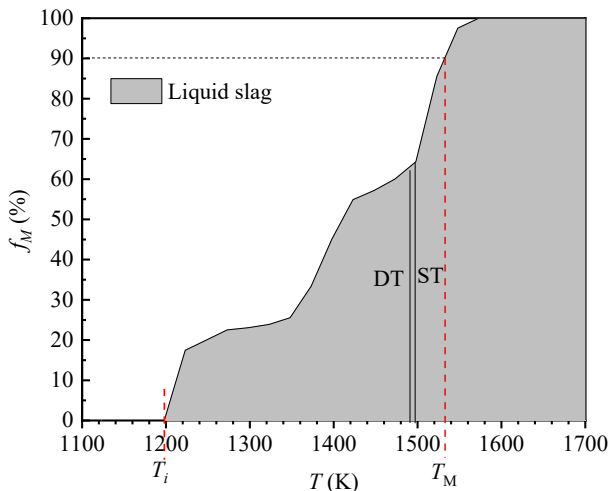


Fig. 2. Liquid fraction curve of Shenhua coal ash.

• Case 1 ($T_i < T_p < T_M$)

Under this condition, the ash is partially melted. The dispersed molten ash adheres to the surface of the particles and finally wraps the char particles (Fig. 1(b) and (c)). The melting ash content mainly controls the particle adhesion, and this muffin mode increases the surface melting ratio of the particles, which is more conducive to particle adhesion. Therefore, the relationship between adhesion probability and ash content should not be linear. Moreover, according to Liu's research [20], the evolution of carbon with reaction time follows an exponential behavior. Thus, it is reasonable to assume that the ash content has a similar exponential trend. The related adhesion probability can be expressed as:

$$f_{c,1} = 1 - \exp(-Bv_a) \quad (3)$$

where the volume fraction of ash v_a is an independent variable (Fig. 4), which can be expressed as:

$$v_a = \frac{a}{\rho_r c + a} \quad (4)$$

where c and a are the residual carbon mass fraction and the ash mass fraction of particle, respectively, and ρ_r is the density ratio of ash to carbon. If $a = 10\%$ in the initial char, the ash density is roughly ten times larger than carbon [19]; thus, 10 can be set here. B is the model coefficient and can be -4.6 (when $a = 1, f = 0.99$).

Assuming that the conservation of ash is existed in the particle before and after the reaction, the carbon conversion X of the particle can be expressed as:

$$X = \left(1 - \frac{cA}{(1-c)C}\right) = \left(1 - \frac{cA}{aC}\right) \times 100\% \quad (5)$$

where C is the carbon content (in mass fraction) in the raw coal, A is the ash content (in mass fraction) in the raw coal. The particle adhesion probability can be expressed as a function of the carbon conversion rate by combining Eqs. (3)-(5):

$$f_{c,1} = 1 - \exp\left(\frac{-4.6A}{C(1-X)\rho_r + A}\right) \quad (6)$$

• Case 2 ($T_p \geq T_M$)

When the particle's temperature is greater than T_M , ash is completely melted with fluidity, concentrates due to surface tension, and is hard to wrap residual carbon. For one case, the molten ash is probably separated from the carbon (Fig. 5). Therefore, it can be assumed that the adhesion probability of the particles is proportional to the volume of the molten ash:

$$f_{c,2,1} = v_{ash} = \frac{a}{\rho_r c + a} \quad (7)$$

For another case, when the content of the molten ash accounts for the majority, it starts to concentrate at the surface of the residual carbon, and gradually forms droplets. Finally, the residual carbon will float on the surface of the molten ash droplet (Fig. 3(d)). A new model needs to be developed. Under these circumstances, the residual carbon volume will mainly determine the probability of adhesion, and it may be assumed that when the residual carbon mass fraction is reduced to $<50\%$, the molten ash accumulation area begins to form. The rebound capacity is equal to the ratio of residual carbon to ash content. Hence, the adhesion probability can be expressed as:

$$f_{c,2,2} = 1 - \frac{c}{a} (c \leq a) \quad (8)$$

According to the above formula, the adhesion probability increases

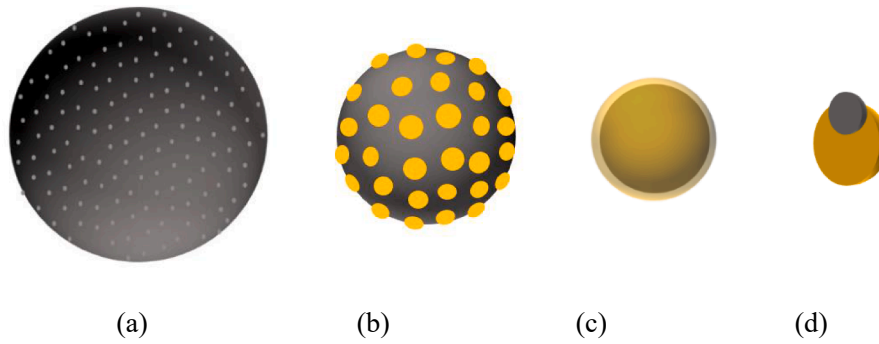


Fig. 3. Char-slag interaction models: (a) Plum pudding mode, (b) Muffin mode, (c) Watermelon mode, (d) Iceberg mode [20,21].

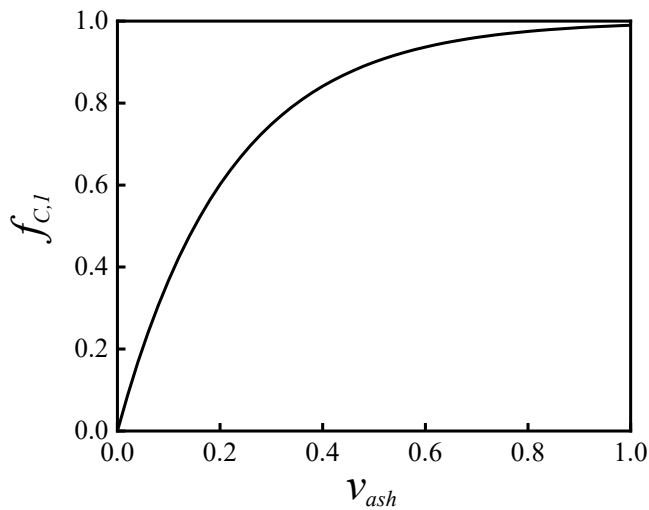


Fig. 4. Exponential relationship between ash volume and adhesion probability.

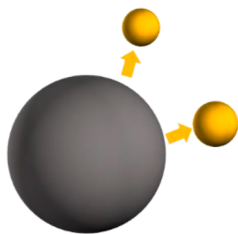


Fig. 5. Separation of the molten ash from residual carbon.

with decreasing carbon content. When the carbon residue accounts for 50% (i.e., $c = 50\%$), the adhesion probability is 0.

The two models (Eqs. (7) and (8)) jointly determine the adhesion probabilities of the particles with different degrees of conversion at a temperature greater than T_M . Thus, it can be expressed as:

$$f_{C,2} = \max\left(\frac{a}{\rho_r c + a}, 1 - \frac{c}{a}\right) \quad (9)$$

The relationship with carbon conversion rate is:

$$f_{C,2} = \max\left(\frac{A}{C(1-X)\rho_r + A}, 1 - \frac{(1-X)C}{A}\right) \quad (10)$$

Combining Eqs. (4) and (8) results in:

$$f_c = \begin{cases} 1 - \exp\left(\frac{-4.6A}{C(1-X)\rho_r + A}\right) & (T < T_M) \\ \max\left(\frac{A}{C(1-X)\rho_r + A}, 1 - \frac{(1-X)C}{A}\right) & (T \geq T_M) \end{cases} \quad (11)$$

The distribution of ash on the particle surface is attributed to the influence of adhesion; therefore, the adhesion probability can be expressed as the intersection of this factor and the ash fusion fraction. The structure of the particle changes significantly, as its surface is not covered by ash. Hence, the influence of ash melting fraction on the adhesion probability can be ignored when the temperature is greater than T_M . In summary, the adhesion sub-model based on the surface characteristics can be expressed by:

$$p_s = \begin{cases} f_M f_c & T_i \leq T_p < T_M \\ f_c & T_p \geq T_M \end{cases} \quad (12)$$

2.1.2. Adhesion model based on the particle kinetic parameters

Particle adhesion is the process in which the particle's kinetic energy is not sufficient to overcome the adhesion force. Hence, the kinetic energy parameters can be used to determine the upper and lower limits of the particle adhesion propensity. The solid particles and liquid particles are considered separately according to T_i .

(1) $T_p < T_i$

Under this condition, the particles are considered solid. The adhesion force between the particles is van der Waals force; therefore, the critical velocity model based on the JKR impact theory of the solid particles is adopted [22]. In addition, for the particles adhered to the wall, the particles will roll away when the fluid shear moment is greater than the adhesion moment. This indicates that the fluid has a critical shear velocity. The kinetic energy parameter criterion can be expressed as:

$$p_K = \begin{cases} 1 & u_p \leq u_{cr} \ \&\& \ u_{g,\tau} \leq u_{\tau c} \\ 0 & u_p > u_{cr} \ \parallel \ u_{g,\tau} > u_{\tau c} \end{cases} \quad (12)$$

where u_{cr} is the critical velocity for particle, $u_{g,\tau}$ is the wall shear velocity of the gas, $u_{\tau c}$ is the critical shear velocity. Detailed formulations and calculations are shown in the supplementary section.

(2) $T_p > T_i$

Under this condition, partial or full melting of the particles occurs, and the adhesion force becomes surface tension. According to Bennett [26], when the droplet impacts the wall, the spreading of the particles will be jointly affected by surface tension and viscous dissipation. When the following criteria are met, the spreading will be completely dominated by surface tension, and the viscous dissipation can be ignored. Therefore, Eq. (13) can be used as a criterion for applying the corresponding surface tension model.

$$We < 2.8Re^{0.457} \quad (13)$$

where $We = \frac{\rho_p u_p^2 d_p}{\gamma_p}$, and Re is the particle Reynolds number.

Generally, the particles will stick until their kinetic energy is sufficient to overcome the effects of viscosity and surface tension [11,14]. Therefore, the maximum kinetic energy that meets the adhesion criterion can be defined as the critical kinetic energy, $E_{k,c}$, as expressed below:

$$E_{k,c} = \begin{cases} E_{k,c,\mu} & We \geq 2.8Re^{0.457} \\ E_{k,c,\gamma} & We < 2.8Re^{0.457} \end{cases} \quad (14)$$

where $E_{k,c,\mu}$ and $E_{k,c,\gamma}$ represent the critical kinetic energy corresponding to viscosity and surface tension effects, respectively. p_K can be obtained by comparing the particle kinetic energy with the critical kinetic energy.

$$p_K = \begin{cases} 1 & E_k \leq E_{k,c} \text{ or } |u_p| \leq u_{cr} \text{ and } |u_{g,\tau}| \leq u_{\tau c} \\ 0 & E_k > E_{k,c} \end{cases} \quad (15)$$

The detailed model for $E_{k,c,\mu}$ and $E_{k,c,\gamma}$ are derived as follows.

- Critical kinetic energy corresponding to the viscosity

Kleinhan's binary critical viscosity model is used to calculate the critical kinetic energy corresponding to the viscosity [11]. $E_{k,c,\mu}$ can be expressed as a function of the particle viscosity μ_p and impact angle :

$$E_{k,c,\mu}^{-1.78} = 5 \cdot 10^{-12} \cdot \mu_p^{-1} \cdot 10^{-6.36/\tan(\varphi)^{0.25}} \quad (16)$$

μ_p is calculated by viscosity-temperature curve, as shown in Eq. (30).

- Critical kinetic energy corresponding to the surface tension

As the ash particles hit the wall without severe deformation [11], the process of the ash droplet impacting the wall can be simplified (Fig. 6). It is assumed that the droplet impact deformation is controlled by surface tension only, and the droplet remains in the initial spherical shape after rebounding.

Before the particles impact the wall, the energy of the particles includes the kinetic energy and surface tension energy :

$$E_1 = E_k + E_s \quad (17)$$

It is assumed that the energy of the rebound particles exists after droplet impacting, which includes the surface tension energy and residual kinetic energy e . Hence, the particle kinetic energy mainly overcomes the adhesion work W during impact:

$$E_2 = E_s + e \quad (18)$$

$$E_1 - E_2 = E_k - e = W \quad (19)$$

The maximum spread diameter of the droplet is d_M . Assuming that

the radius of the contact surface is r , the adhesion work W can be expressed as:

$$W = \frac{\pi}{4} (d_M)^2 \sin^2 \theta \gamma_{lv} (1 + \cos \theta) \quad (20)$$

where γ_{lv} is the surface tension of the particle, as determined by ash composition and temperature in Eq. (31). The maximum spreading ratio of the particles [14]:

$$\xi_m = \frac{d_M}{d_p} = 1 + 0.259We^{0.317} \quad (21)$$

The contact angle θ is set to 120° [1]. The critical kinetic energy is equivalent to adhesion work, by combining Eqs. (20) and (21):

$$E_{k,c} = W = \frac{\pi}{4} (d_p \xi_m)^2 \sin^2 \theta \gamma_{lv} (1 + \cos \theta) \quad (22)$$

In addition, the effect of fluid shear force on particle adhesion is determined. Combined with Eq. (20) and moment balance calculation [27], it is estimated that when the particle size is $100 \mu\text{m}$, the critical shear velocity is $> 30 \text{ m/s}$ (entrained-flow gasification condition, $> 300 \text{ m/s}$ in combustion furnaces), which is much greater than the gas velocity near the wall. Therefore, when the particles are liquid or semi-liquid, the influence of gas velocity on particle adhesion can be ignored.

2.1.3. Proposal of the particle adhesion model

In summary, the particle adhesion model can be classified according to T_i . When $T_p < T_i$, only the adhesion criterion corresponding to the kinetic energy parameter needs to be considered. Otherwise, the particle's surface characteristics and kinetic energy parameters should be considered simultaneously, and the adhesion probability of the particle is the intersection of the two factors. The adhesion model based on the coal particle surface characteristics could be given by Eq. (23)

$$P_p = \begin{cases} p_K & T_p < T_i \\ p_K p_S & T_p \geq T_i \end{cases} \quad (23)$$

Since P_K is a Boolean criterion, the model can be transformed into a flow chart (Fig. 7). The critical velocity of the particles are considered primarily

2.2. Comprehensive adhesion model with slag layer

In coal combustion and gasification on the furnace, there is a slag layer or deposit on the wall; thus, the influence of the furnace wall properties on particle/droplet adhesion probability should also be considered. The influence of the slag layer on the adhesion probability is mainly reflected in the interaction between the particles and slag layer. Hence, the physical properties of slag layer are essential, especially viscosity and surface tension.

When the surface slag layer temperature is higher than T_i , the slag

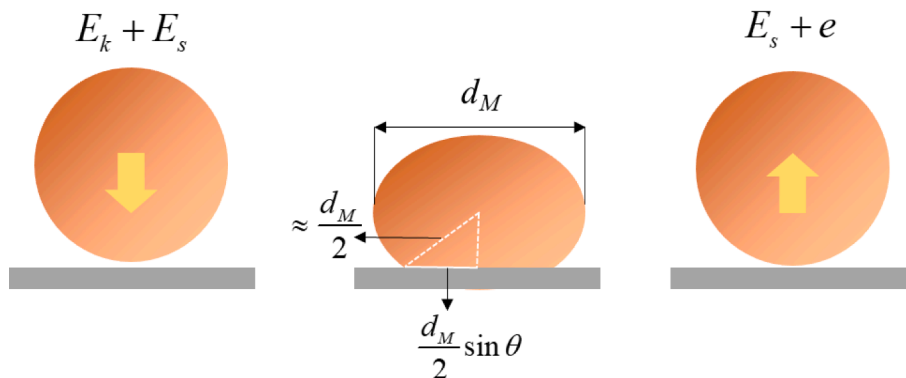


Fig. 6. Simplified process of the droplets hitting the wall.

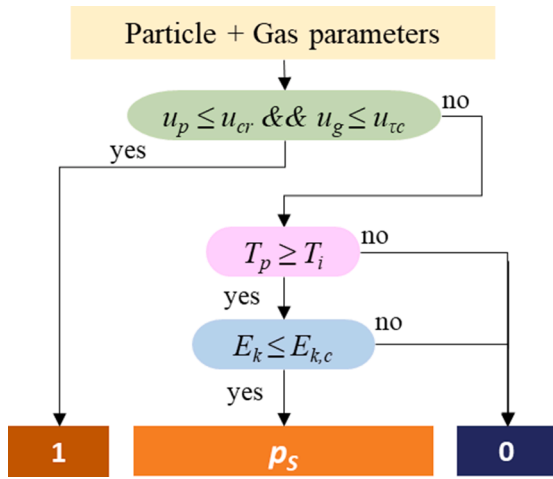


Fig. 7. Flowchart of particle adhesion model.

layer is considered to have a more significant impact on particle deposition, regardless of the influence of the slag layer/deposited layer at lower temperatures. Thus, the slag layer can be assumed as a liquid film. For the particle impingement on the liquid film, the capillary number Ca can be used to compare the magnitude of the two effects [28].

$$Ca = \frac{\mu_{film} u_p}{\gamma_{film}} \quad (24)$$

The order of magnitude of the surface tension of the slag layer is 10^{-1} , which is usually less than or equal to the order of magnitude of the particle velocity, while the order of magnitude of the viscosity of the slag layer is usually more than 10^1 . Therefore, for most cases in the combustion furnace and gasifier, $Ca > 1$, the viscosity of plays a dominant role, and the influence of the surface tension of the slag layer can be temporarily ignored.

The critical viscosity model based on the particle kinetic energy is adopted [11].

$$p_{\mu,w} = \begin{cases} 0 & \mu_w > \mu_{p,c} \\ 1 & \mu_w \leq \mu_{p,c} \end{cases} \quad (25)$$

where $\mu_{p,c}$ is the critical viscosity of the particle, which can be calculated from the relation of particle kinetic energy, according to Eq. (16). The slag compositions vary by conditions and difficult to predict quantitatively. [29] Since particle adhesion is only affected by the surface of the slag layer, it can be assumed as the same composition as the particles.

The melting fraction of the slag layer could be expressed as: $f_{M,w}=F(T_{wall})$, similar with the particles. Then, the adhesion probability of the slag layer can be expressed as:

$$P_w = p_{\mu,w} f_{M,w} \quad (26)$$

Combined with the particle adhesion model proposed in Section 2.1, the particle comprehensive adhesion probability is expressed as:

$$P_T = 1 - (1 - P_p)(1 - P_w) \quad (27)$$

The primary input parameters required by each probability model are summarized in Fig. 8.

3. Model validation and discussion

3.1. Model validation

3.1.1. Validation of the particle deposition under gasification conditions

As discussed above, when the temperature of the particle is greater than T_i , p_s will control particle adhesion (no slag layer as a precondition). To verify this model, a modeling study is carried out according to Li's deposition experiment of gasified char particles at different carbon conversion rates [6]. In Li's experiment, a drop tube furnace was adopted as the reactor, where an inclined plate placed at the bottom of the furnace was set as a deposition surface. Moreover, no slag layer or deposit is formed. Illinois No. 6 coal is selected as a raw material, and its composition is shown in Table 1. Ash melting fraction curve is calculated by FactSage (Fig. 9).

The specific structure and kinetic parameters are detailed in Li and Whitty [6]. Since there is no formation of slag or deposit, P_w is considered as 0. Assuming that the velocity of the particles is equal to

Table 1
Parameters required for verification.

Raw coal composition(wt.%)		Ash composition, (wt.%d)	
<i>Proximate analysis</i>			
Moisture	3.63	SiO ₂	46.58
Ash	10.89	Al ₂ O ₃	17.75
Volatile matter	36.42	TiO ₂	0.88
Fixed Carbon	52.69	Fe ₂ O ₃	18.99
<i>Ultimate analysis</i>			
Carbon	74.48	MgO	0.89
Hydrogen	4.92	CaO	5.23
Nitrogen	1.48	Na ₂ O	1.67
Sulfur	4.66	K ₂ O	2.06
Furnace temperature	1673 K; 1773 K	P ₂ O ₅	0.16
		SO ₃	4.59

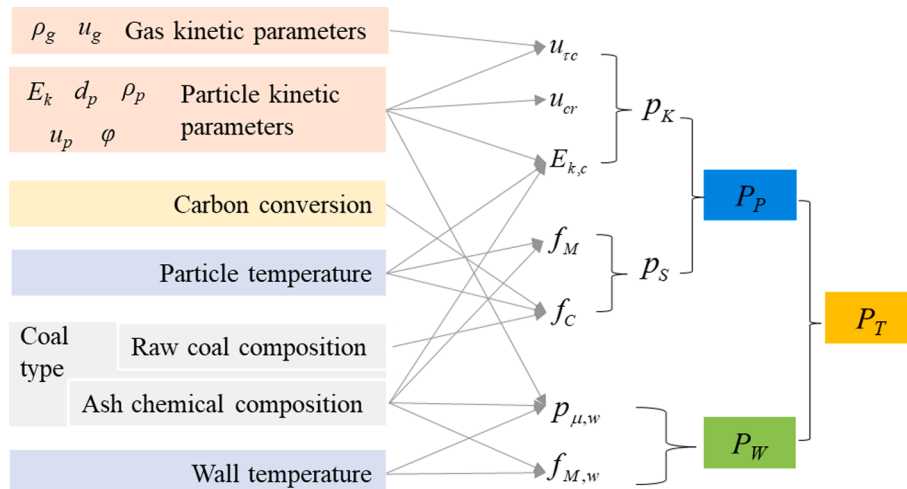


Fig. 8. The main input parameters of each adhesion model.

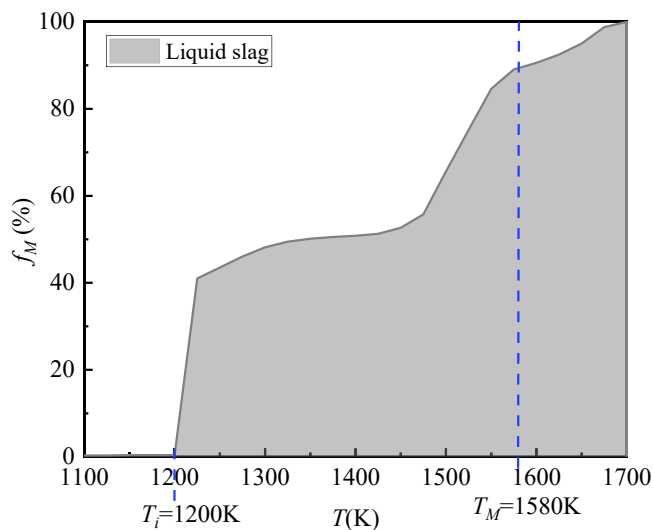


Fig. 9. Melting fraction curve of the coal used in Li [6].

the gas velocity, the calculations show that all the velocities of the particles when they contact the wall are greater than the critical velocity, and do not exceed the critical kinetic energy required for rebounding. Therefore, the adhesion probability of the particles is dependent on the p_s . According to Table 1 and Fig. 9, both two furnace temperatures are higher than T_M , so particle adhesion is dependent on .

Fig. 10 shows that the predicted particle adhesion probability increases slowly at low conversion and increases sharply at high conversion. Interestingly, the adhesion probability trend of this model is in good agreement with the experiment.

3.1.2. Local simulation of the combustion furnace

To verify the model’s reliability at lower temperatures, a local simulation of furnace particle deposition is carried out. According to the deposition experiment data of the 15 kW descending combustion furnace in Beckmann’s research [30], a similar two-dimensional model is constructed by selecting the position of Port3 in the laminar flow state according to Yang’s simulation [14], as shown in Fig. 12. The parameters of the coal and two simulation conditions (uncooled probe and cooling probe) are shown in Tables 2 and 3. Middelburg coal is used in the experiment, and its ash melting fraction curve calculated by

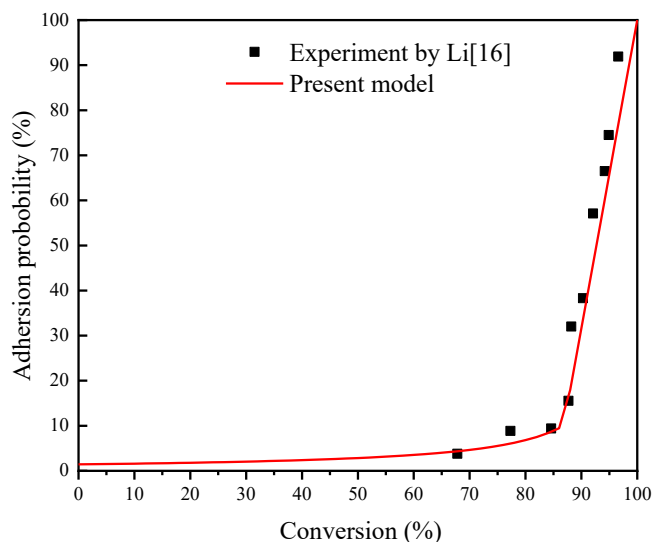


Fig. 10. Particle adhesion efficiency predicted by the present model.

Table 2 Parameters for the two simulation conditions.

Probe type	Port3	
	uncooled	cooled
Surface temperature, K	1398	873
<i>Furnace condition</i>		
Gas velocity, m/s	0.36	
Gas temperature, K	1398	
O ₂ , vol%	0.37	
CO ₂ , vol%	15.70	
<i>Particle properties</i>		
Size distribution, μm	Rosin-Rammler, d_{mean} (20), n (0.80)	
Particle loading on project area, g/h	19.83(ash) + 0.98(combustibles)	
Density, kg/m ³	2600 (ash); 500 (combustibles)	
Conversion (Burnout),%	99.41	
Specific capacity, J/(kg K)	975.65 + 0.23 × T	

Table 3 Composition of the coal.

Raw coal composition(wt.%)	Ash composition, (wt.%)	
<i>Proximate analysis</i>		
Moisture	6.11	SiO ₂ 37.3
Ash	9.97	Al ₂ O ₃ 28.9
Volatiles matter	30.4	TiO ₂ 1.3
Fixed Carbon	53.52	Fe ₂ O ₃ 5.8
<i>Ultimate analysis</i>		
Carbon	66.22	MgO 3.2
Hydrogen	4.04	CaO 11.0
Nitrogen	1.75	Na ₂ O 1.5
Sulfur	0.87	K ₂ O 1.2
		P ₂ O ₅ 1.7
		SO ₃ 8.1

FactSage is shown in Fig. 11, which can be reduced to a piecewise function. It can be seen that the furnace temperature is between T_i and T_M , while the temperature of the cooled wall is lower than T_i .

The simulation region of the flow field is 0.3 m × 0.6 m, and the deposition probe with a diameter of 22 mm is located at the center. The mesh width near the probe is about 0.25 mm, which meets the mesh packing requirements of Weber [31].

To simulate the gas phase turbulence flow in the furnace, the time-averaged steady-state Navier-Stokes equations, as well as the energy conservation of gas species transport equations, The Realizable k-ε model and the Enhanced Wall model are used. DO radiation model realizes the radiation heat transfer; DPM model is used for particle/droplet tracking, by considering both gravity and thermophilic force; and the chemical reaction can be ignored.

The particle deposition model is added to Fluent via user-defined

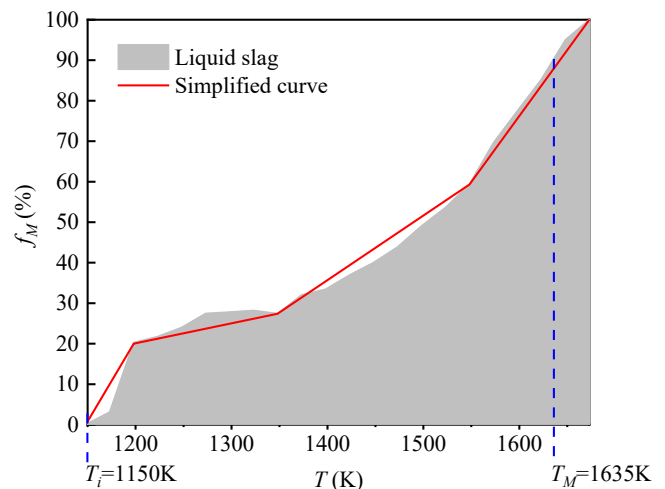


Fig. 11. Melting fraction of the Middelburg coal ash and simplified curve.

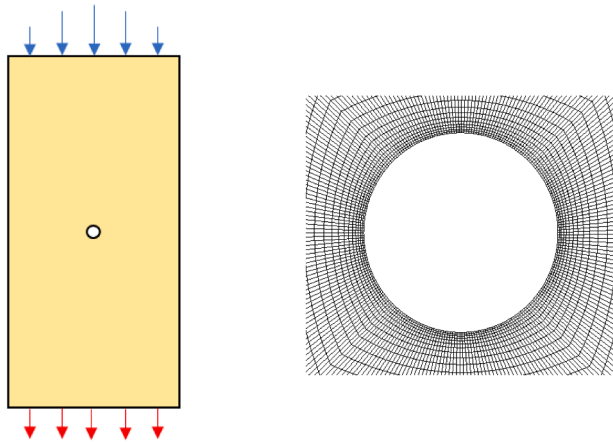


Fig. 12. Two-dimensional model and the fine mesh near the deposition probe.

functions (UDF), according to the model described in Section 2. DEFINE_DPM_BC is used to Achieve particle adhesion and rebound; and DEFINE_DPM_EROSION realizes the calculation of the deposition rate.

Particle parameters setting: Particle loading at the inlet is distributed according to the mass flux. For considering the residual carbon in the ash particles, two substances are injected simultaneously according to the mass ratio of residual carbon to ash, to simulate different particle properties under the actual conditions. The particle size distribution is obtained by fitting the measured data with the rosin-rammer distribution and maintaining uniform. In addition, the temperature of the impact particles varies with size for those >80 μm, while the smaller particle temperature depends on deposition surface temperature conditions [30]. Thus, the temperature of large particles is amended fitting relation as the entrance particle parameters.

To verify the simulation accuracy of the local simulation, the particle impact rate of the model was compared with the impact rate of the three-dimensional global simulation from Beckmann [30] (Fig. 13). The maximum difference in particle impact rates between local simulation and global simulation is 5%, which appears to be relatively close. Therefore, the two-dimensional local simulation can be used to predict the particle deposition rate.

Fig. 14 shows that the particle deposition rate predicted by the proposed model is close to the experimental data, as calculated by: impact rate × P_T . The prediction rates of the other two adhesion models

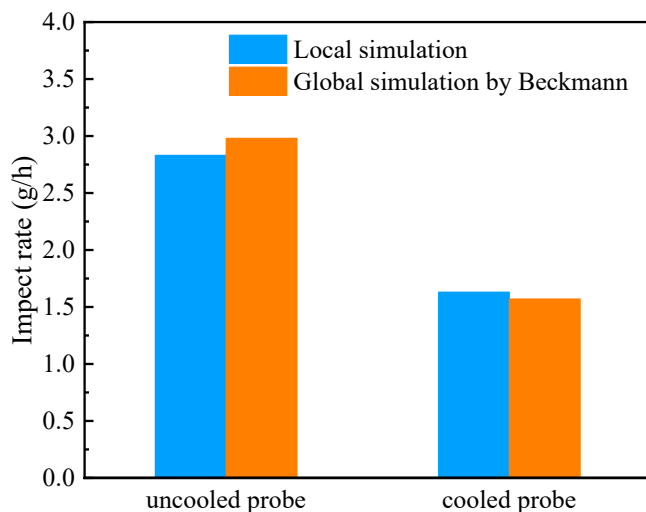


Fig. 13. Comparison of impact rate between local simulation and global simulation [27].

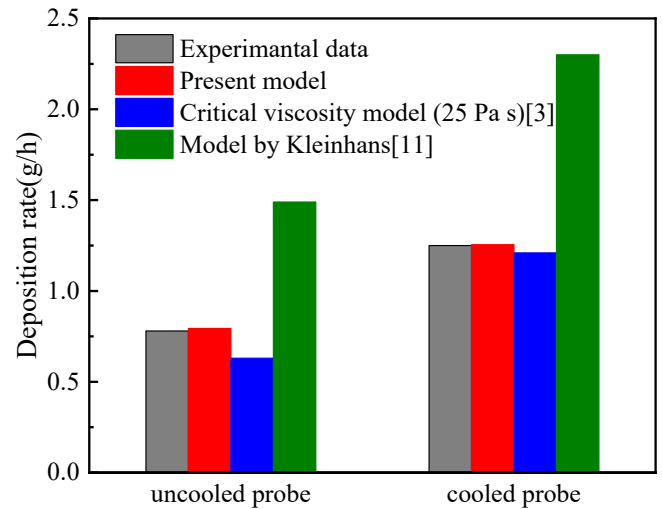


Fig. 14. Comparison of the deposition rate predicted by the model and experimental data.

were compared. As shown in Fig. 13, the present model is greatly improved over Kleinhans' model, and more accurate than the critical viscosity model, under the uncooled surface conditions.

3.2. Discussion

3.2.1. Effect of particle kinetic parameters on particle adhesion propensity

As shown in Fig. 7, particle adhesion is limited by the kinetic energy parameters of particle and gas, namely P_K . Here, the influence of particle kinetic energy on adhesion ability is mainly considered.

Taking SH coal as an example ($T_i = 1200$ K, $T_M = 1530$ K), its viscosity is obtained by fitting the viscosity-temperature curve measured by the experiment:

$$\lg \mu_p (\text{Pa}\cdot\text{s}) = -9.892 + \frac{16971.1}{T(K)} \quad (30)$$

The surface tension is calculated using the relational formula with temperature, and the surface tension of 1300°C is calculated according to the composition of coal ash [33]. Considering that the surface tension of coal ash will increase suddenly at lower temperatures, 1000 mN/m is taken when the temperature is lower than 1300°C [34].

$$\gamma_p (\text{mN/m}) = \begin{cases} 423.8 + 0.004 \cdot (T - 1573) & T > 1573\text{K} \\ 1000 & \text{else} \end{cases} \quad (31)$$

The particle density is given as 1500 kg/m³, the particle size is 50 μm, and the impact angle is 60°. The particle kinetic energy varies by changing the particle velocity. By default, the gas velocity is less than the critical shear velocity.

As shown in Fig. 15, the adhesion area can be divided into three zones:

- 1) Adhesion zone: When E_k is very low, the particles will adhere because the velocity is less than the critical velocity; for those with temperatures close to T_i , the adhesion of the particles will be almost determined by the critical velocity model.
- 2) Probability zone: E_k is less than the critical kinetic energy, and the temperature of particles is higher than T_i . At this point, the kinetic energy can be considered in medium range, the adhesion propensity of the particles is expressed by .
- 3) Rebound zone: When E_k is further increased and more significant than the critical kinetic energy, the viscosity or surface tension effect is overcome. Thus, the physical property determines whether the particle rebound or not.

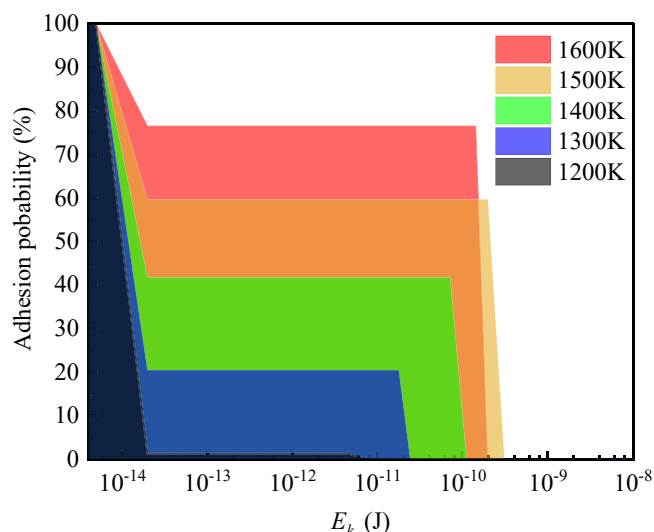


Fig. 15. The relationship between particle kinetic energy and adhesion area at different temperatures (the carbon conversion is set to 0.9).

The relationship between particle adhesion and kinetic energy is simplified in Fig. 16.

The temperature in the furnace is mostly higher than T_i , so the particle rebound is dependent on the critical kinetic energy corresponding to the viscosity and surface tension, which can be divided by the particle kinetic energy becoming a dimensionless number $E_{k,c}^*$ (Fig. 17). $E_{k,c}^*$ decreases with increasing particle velocity, suggesting that the particles with small kinetic energy tend to stick after impact. With an increase in the temperature of the particles, the range of velocity for adhesion gradually increases, indicating that more adhesion occurs in higher temperatures, and the critical kinetic energy corresponding to the two effects of surface tension and viscosity remains almost consistent.

3.2.2. Effect of particle surface characteristics on particle adhesion propensity

The above analysis shows that the adhesion propensity is dependent on P_s , when the particle kinetic energy is within the medium range. As shown in Fig. 8, the surface characteristics model can be summed up in three parameters: coal types, particle temperature and carbon conversion.

(1) Influence of the ash-carbon ratio

For the slagging gasifier with a membrane wall, a high content of ash is required to achieve wall slagging, which is usually implemented by coal blending or slag blending (the slag returns to the coal grinding system).

The particle adhesion probability of different ash-carbon ratios is shown in Fig. 18. It can be found that the probability of adhesion increases with increasing ash-carbon ratio ($r_{a/c}$). In addition, the mutation points of the adhesion probability corresponding to the carbon conversion decrease with increasing ash-to-carbon ratio. This means that, for slagging gasifier, a high ash-carbon ratio of the input material leads to an increased deposition, which can be conducive to liquid slagging.

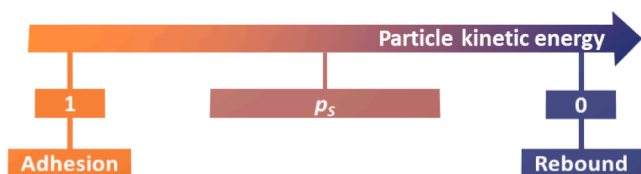


Fig. 16. Schematic of the particle kinetic energy and adhesion.

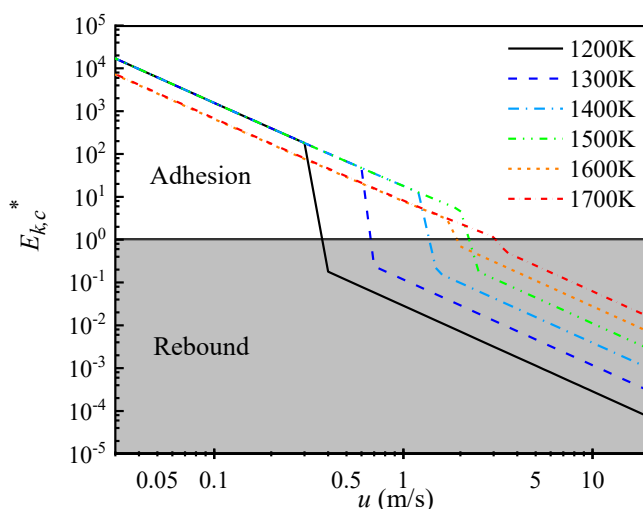


Fig. 17. The relationship between particle velocity and $E_{k,c}^*$ at different temperatures.

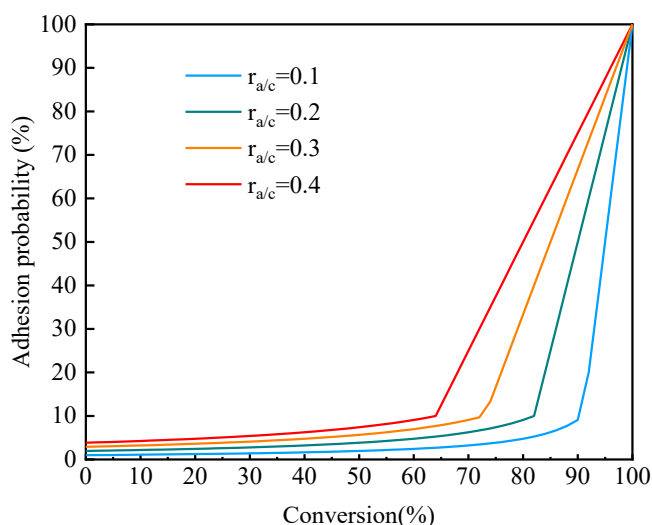


Fig. 18. The relationship between carbon conversion rate and adhesion probability at different coal ($T_p > T_M$).

(2) Influence of particle temperature and conversion

In the gasifier, it is generally believed that the particle temperature is basically balanced with the local gas temperature (for $d_p < 100 \mu m$, the temperature relaxation time of coal $< 0.01 s$ generally), so the temperature of the particles also reflects the local temperature.

With fixing coal composition, the relationship between the conversion rate of particulate carbon and adhesion probability at different temperatures is shown in Fig. 19 (take Middelburg coal as an example, $T_i = 1150 K$, $T_M = 1640 K$):

When the temperature is close to T_i , the particle adhesion probability increases slowly with increasing carbon conversion, and gradually raises at higher temperatures. When the temperature is higher than T_M , the probability of particle adhesion will increase sharply at high carbon conversion. Since the adhesion probability directly reflects the surface characteristics of the particles, the tendency is consistent with the morphological characteristics of the particles observed in the experiment of Li and Whitty [32]. In particular, the morphological changes in the particles at lower temperatures are not found during the conversion process; while at higher temperatures, an obvious morphological

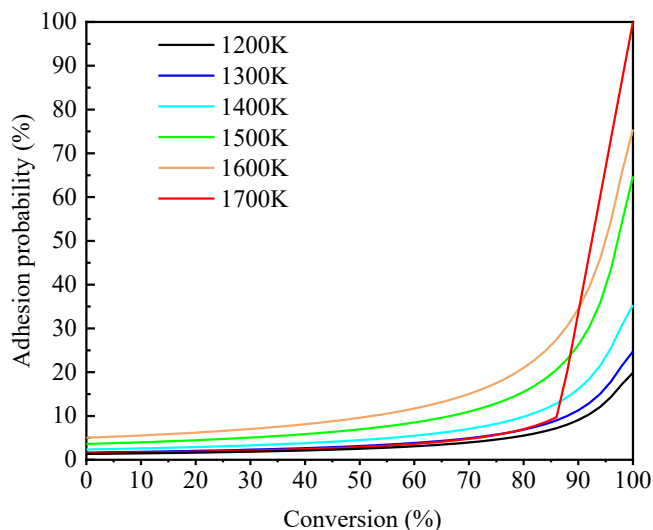


Fig. 19. The relationship between carbon conversion rate and adhesion probability at different temperatures.

difference was observed between low conversion and high conversion states.

As shown in Fig. 20, when the temperature is higher than T_M , the adhesion probability of the particles remains constant at different temperatures, which is consistent with the experimental results of Li's capture efficiency for high-temperature gasification particles. Meanwhile, when the carbon conversion is lower, the particles below T_M appear to have a higher adhesion probability than those in higher temperatures, indicating that the more solid structures of the particle surface emerge at high temperatures. The findings on the evolution of the particle surface area confirm this phenomenon [32].

For combustion furnaces, the aim is to suppress ash accumulation, and the temperature distribution range is wide, ranging from below T_i to above T_M . Under the conditions of low temperature and high speed, ash deposition can be restrained. Another way is to change the composition of the raw materials by increasing T_i . For the entrained-flow gasifier, ash deposition should be promoted to achieve liquid slagging, and the temperature is usually higher than T_M . In other words, when the critical kinetic energy of the particles is higher, the probability zone is larger, making them more difficult to rebound. Under the same slag layer condition, carbon conversion is the main factor that affects the adhesion propensity of the particles. These data suggest that a prolonged residence time is conducive to ash deposition and liquid slagging.

4. Conclusion

A comprehensive model of particle adhesion suitable for combustion and gasification process is proposed based on the surface characteristics analysis, by considering ash ratio and melting fraction. Moreover, two validation sets at high and low temperatures have proved the effectiveness of the model in predicting the probability of particle adhesion. This model quantitatively describes the relationship between the carbon conversion and particle adhesion, which provides a solution for further accurately predicting the particle deposition rate of combustion furnaces and gasifiers under different operating conditions. However, this model ignores some factors such as the influence of solid slag properties or deposition on adhesion propensity and the heterogeneity of ash distribution in particles, which require to be further explored.

The model shows that, when the particle kinetic energy is greater than the critical velocity and lower than the critical kinetic energy, the surface characteristics play an important role on adhesion propensity, which can be determined by components, temperature, and particle conversion. The adhesion probability is greater when the ash-carbon

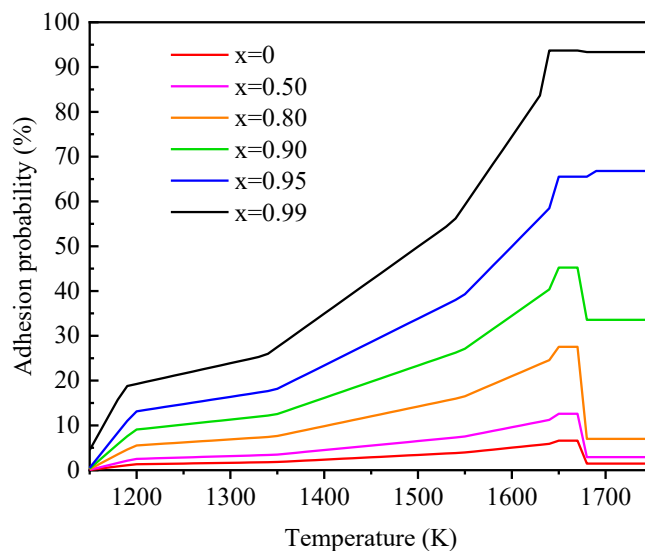


Fig. 20. The relationship between temperature and adhesion probability at different carbon conversion rates.

ratio is higher. With the increase in carbon conversion, the adhesion probability first increases gradually and then rises sharply. With the increase in temperature, the critical kinetic energy and ash melting fraction increase, indicating a high adhesion propensity for the particles.

CRediT authorship contribution statement

Fanfei Lin: Investigation, Methodology, Data curation, Writing – original draft. **Zhongjie Shen:** Visualization. **Qinfeng Liang:** Formal analysis. **Zhenghua Dai:** Methodology. **Jianliang Xu:** Software, Supervision, Writing – review & editing. **Haifeng Liu:** Conceptualization, Supervision.

Declaration of Competing Interest

The authors declare that they have no known competing financial interests or personal relationships that could have appeared to influence the work reported in this paper.

Acknowledgements

This work was supported by the Shanghai Outstanding Technology Leader [Grant number 19XD1434800] and the National Natural Science Foundation of China [Grant number 21878082, 21776087].

The authors would like to express their gratitude to EditSprings (<https://www.editsprings.cn/>) for the expert linguistic services provided.

References

- [1] Xu J, Dai Z, Liu H, Guo L, Sun F. Modeling of multiphase reaction and slag flow in single-burner coal water slurry gasifier[J]. Chem Eng Sci 2017;162:41–52.
- [2] Troiano M, Solimene R, Montagnaro F, Salatino P. Char/ash deposition and near-wall segregation in slagging entrained-flow gasification of solid fuels: from experiments to closure equations[J]. Fuel 2020;264:116864. <https://doi.org/10.1016/j.fuel.2019.116864>.
- [3] Walsh PM, Sayre AN, Loehden DO, Monroe LS, Beér JM, Sarofim AF. Deposition of bituminous coal ash on an isolated heat exchanger tube: effects of coal properties on deposit growth[J]. Prog Energy Combust Sci 1990;16(4):327–45.
- [4] Naruse I, Kamihashira D, Miyauchi Y, Kato Y, Yamashita T, Tominaga H. Fundamental ash deposition characteristics in pulverized coal reaction under high temperature conditions[J]. Fuel 2005;84(4):405–10.
- [5] Akiyama K, Pak H, Tada T, Ueki Y, Yoshiie R, Naruse I. Ash deposition behavior of upgraded brown coal and bituminous coal[J]. Energy Fuels 2010;24(8):4138–43.
- [6] Li S, Wu Y, Whitty KJ. Ash deposition behavior during char-slag transition under simulated gasification conditions[J]. Energy Fuels 2010;24(3):1868–76.

- [7] Cai Y, Tay K, Zheng Z, Yang W, Wang H, Zeng G, et al. Modeling of ash formation and deposition processes in coal and biomass fired boilers: A comprehensive review [J]. *Appl Energy* 2018;230:1447–544.
- [8] Mueller C, Selenius M, Theis M, Skrifvars B-J, Backman R, Hupa M, et al. Deposition behaviour of molten alkali-rich fly ashes—development of a submodel for CFD applications[J]. *Proc Combust Inst* 2005;30(2):2991–8.
- [9] Mao T, Kuhn DCS, Tran H. Spread and rebound of liquid droplets upon impact on flat surfaces[J]. *AIChE J* 1997;43(9):2169–79.
- [10] Ni J, Yu G, Guo Q, Zhou Z, Wang F. Submodel for predicting slag deposition formation in slagging gasification systems. *Energy Fuels* 2011;25(3):1004–9.
- [11] Kleinhans U, Wieland C, Frandsen FJ, Spliethoff H. Ash formation and deposition in coal and biomass fired combustion systems: Progress and challenges in the field of ash particle sticking and rebound behavior[J]. *Prog Energy Combust Sci* 2018; 68:65–168.
- [12] Kleinhans U, Wieland C, Babat S, Scheffknecht G, Spliethoff H. Ash particle sticking and rebound behavior: A mechanistic explanation and modeling approach[J]. *Proc Combust Inst* 2017;36(2):2341–50.
- [13] Brink A, Lindberg D, Hupa M, de Tejada ME, Paneru M, Maier J, et al. A temperature-history based model for the sticking probability of impacting pulverized coal ash particles[J]. *Fuel Process Technol* 2016;141:210–5.
- [14] Yang X, Ingham D, Ma L, Troiano M, Pourkashanian M. Prediction of particle sticking efficiency for fly ash deposition at high temperatures[J]. *Proc Combust Inst* 2019;37(3):2995–3003.
- [15] Zhou M-M, Parra-Álvarez JC, Smith PJ, Isaac BJ, Thornock JN, Wang Y, et al. Large-eddy simulation of ash deposition in a large-scale laboratory furnace[J]. *Proc Combust Inst* 2019;37(4):4409–18.
- [16] Zhou H, Hu S. Numerical simulation of ash deposition behavior with a novel erosion model using dynamic mesh[J]. *Fuel* 2021;286:119482. <https://doi.org/10.1016/j.fuel.2020.119482>.
- [17] Chen L, Yong SZ, Ghoniem AF. Modeling the slag behavior in three dimensional CFD simulation of a vertically-oriented oxy-coal combustor[J]. *Fuel Process Technol* 2013;112:106–17.
- [18] Yong SZ, Gazzino M, Ghoniem A. Modeling the slag layer in solid fuel gasification and combustion—Formulation and sensitivity analysis[J]. *Fuel* 2012;92(1):162–70.
- [19] Xu J, Liang Q, Dai Z, Liu H. Comprehensive model with time limited wall reaction for entrained flow gasifier[J]. *Fuel* 2016;184:118–27.
- [20] Liu M, Shen Z, Liang Q, Xu J, Liu H. Morphological evolution of a single char particle with a low ash fusion temperature during the whole gasification process [J]. *Energy Fuels* 2018;32(2):1550–7.
- [21] Liu M, Shen Z, Liang Q, Xu J, Liu H. New slag–char interaction mode in the later stage of high ash content coal char gasification[J]. *Energy Fuels* 2018;32(11): 11335–43.
- [22] Brach RM, Dunn PF. A mathematical model of the impact and adhesion of microspheres. *Aerosol Sci Technol* 1992;16(1):51–64.
- [23] Zhou Z, Shen Z, Liang Q, Xu J, Liu H. Effect of element content fluctuation on partial melting behavior of coal ash particles[J]. *Fuel* 2020;271:117608. <https://doi.org/10.1016/j.fuel.2020.117608>.
- [24] Zhou Z, Shen Z, Liang Q, Liu H. Sub-particle scale study on the melting behavior of Zhundong coal ash based on the heterogeneous distribution of elements[J]. *Combust Flame* 2020;216:223–31.
- [25] Bale CW, Bélisle E, Chartrand P, Deckerov SA, Eriksson G, Gheribi AE, et al. FactSage thermochemical software and databases, 2010–2016. *Calphad* 2016;54: 35–53.
- [26] Bennett T, Poulikakos D. Splat-quench solidification: estimating the maximum spreading of a droplet impacting a solid surface[J]. *J Mater Sci* 1993;28(4):963–70.
- [27] H. El-Batsh H. Haselbacher Numerical Investigation of the Effect of Ash Particle Deposition on the Flow Field through Turbine Cascades[C] ASME Paper, No. GT-2002-30600, 2002.
- [28] Barnocky G, Davis RH. The effect of Maxwell slip on the aerodynamic collision and rebound of spherical particles. *J Colloid Interface Sci* 1988;121(1):226–39.
- [29] Shen Z, Nikolic H, Caudill LS, Liu K. A deep insight on the coal ash-to-slag transformation behavior during the entrained flow gasification process[J]. *Fuel* 2021;289:119953. <https://doi.org/10.1016/j.fuel.2020.119953>.
- [30] Beckmann AM, Mancini M, Weber R, Seibold S, Müller M. Measurements and CFD modeling of a pulverized coal flame with emphasis on ash deposition[J]. *Fuel* 2016;167:168–79.
- [31] Weber R, Schaffel-Mancini N, Mancini M, Kupka T. Fly ash deposition modelling: Requirements for accurate predictions of particle impaction on tubes using RANS-based computational fluid dynamics. *Fuel* 2013;108:586–96.
- [32] Li S, Whitty KJ. Investigation of coal char–slag transition during oxidation: Effect of temperature and residual carbon[J]. *Energy Fuels* 2009;23(4):1998–2005.
- [33] Rezaei HR, Gupta RP, Wall TF, Miyamae S, Makino K. Modelling the initial structure of ash deposits and structure changes due to sintering. In: Gupta RP, Wall TF, Baxter L, editors. *Impact of Mineral Impurities in Solid Fuel Combustion*. Boston: Kluwer Academic Publishers; 2002. p. 753–66. https://doi.org/10.1007/0-306-46920-0_57.
- [34] Melchior T, Bläsing M, Pütz G, Müller M. Surface tension measurements of coal ash slags under reducing conditions at elevated pressures[J]. *Fuel* 2011;90(1):280–7.